

# CHANGE DETECTION IN MULTI-TEMPORAL DUAL POLARIZATION SENTINEL-1 DATA

Allan A. Nielsen<sup>a</sup>, Morton J. Canty<sup>b</sup>, Henning Skriver<sup>c</sup>, and Knut Conradsen<sup>a</sup>

<sup>a</sup>Technical University of Denmark, DTU Compute – Applied Mathematics and Computer Science  
DK-2800 Kgs. Lyngby, Denmark

<sup>b</sup>Institute of Energy and Climate Research IEK-6, Jülich Research Center  
D-52425 Jülich, Germany

<sup>c</sup>Technical University of Denmark, DTU Space – National Space Institute  
DK-2800 Kgs. Lyngby, Denmark

## ABSTRACT

Based on an omnibus likelihood ratio test statistic for the equality of several variance-covariance matrices following the complex Wishart distribution with an associated  $p$ -value and a factorization of this test statistic, change analysis in a time series of 19 multilook, dual polarization Sentinel-1 SAR data in the covariance matrix representation (with diagonal elements only) is carried out. The omnibus test statistic and its factorization detect if and when change occurs.

<http://www.imm.dtu.dk/pubdb/p.php?6962>.

## 1. INTRODUCTION

Based on work reported in [1], this contribution detects change in a series of 19 Sentinel-1<sup>1</sup> dual polarization (here covariance matrix representation, [2], VV/VH, diagonal only) C-band synthetic aperture radar (SAR) data over Frankfurt Airport.

In earlier publications we have described a test statistic for the equality of two variance-covariance matrices following the complex Wishart distribution with an associated  $p$ -value [3]. We showed their application to bitemporal change detection and to edge detection [4] in multilook, polarimetric SAR data in the covariance matrix representation. The test statistic and the associated  $p$ -value is described in [5] also. In [6] we focused on the block-diagonal case, we elaborated on some computer implementation issues, and we gave examples on the application to change detection in both full and dual polarization bitemporal, bifrequency, multilook SAR data. In [7] the bitemporal change detection problem in polarimetric SAR data is dealt with by means of the Hotelling-Lawley trace statistic.

In [1] we described an omnibus test statistic  $Q$  for the equality of  $k \geq 2$  variance-covariance matrices following the complex Wishart distribution. We also described a factorization of  $Q = \prod_{j=2}^k R_j$  where  $Q$  and  $R_j$  determine if and when a difference occurs. Additionally, we gave  $p$ -values for  $Q$  and  $R_j$ . Finally, we demonstrated the use of  $Q$ ,  $R_j$  and the  $p$ -values to change detection in truly multi-temporal, full polarization SAR data. For more references to change detection in polarimetric SAR data, see [1].

In [1] we applied the methods to a series of airborne EMISAR L-band data. In this paper we apply the methods to Sentinel-1 C-band data. The methods may be applied to other polarimetric SAR data also such as data from ALOS, COSMO-SkyMed, RadarSat-2, TerraSAR-X, and Yaogan.

<sup>1</sup><https://sentinel.esa.int/web/sentinel/missions/sentinel-1>.

## 2. OMNIBUS CHANGE DETECTION METHOD

The Sentinel-1 data are dual polarization. In the covariance matrix representation each pixel at each time point is a matrix

$$\langle \mathbf{C} \rangle_{dual} = \begin{bmatrix} \langle S_{vv} S_{vv}^* \rangle & \langle S_{vv} S_{vh}^* \rangle \\ \langle S_{vh} S_{vv}^* \rangle & \langle S_{vh} S_{vh}^* \rangle \end{bmatrix}.$$

In our case we have the diagonal elements only. The matrix with the off-diagonal elements set to zero does not follow a complex Wishart distribution but the two (1 by 1) “blocks” on the diagonal do [1, 3, 4, 6]. The “block”  $\langle S_{vv} S_{vv}^* \rangle$  is 1 by 1,  $p_1 = 1$ , and the “block”  $\langle S_{vh} S_{vh}^* \rangle$  is 1 by 1,  $p_2 = 1$ .

For the logarithm of the test statistic  $Q$  for no change between all  $k$  time points introduced in [1], we get

$$\ln Q = n \{ pk \ln k + \sum_{i=1}^k \ln |\mathbf{X}_i| - k \ln \left| \sum_{i=1}^k \mathbf{X}_i \right| \}. \quad (1)$$

Here  $p = p_1 + p_2 = 2$  and  $\mathbf{X}_i = n \langle \mathbf{C} \rangle_{dual}$  where  $n$  is the equivalent number of looks.  $|\cdot|$  denotes the determinant.

For the test statistic  $R_j$ , that given no change between the first  $j-1$  time points, we have no change between time points  $j-1$  and  $j$ , we get

$$\begin{aligned} \ln R_j &= n \{ p(j \ln j - (j-1) \ln(j-1)) \\ &+ (j-1) \ln \left| \sum_{i=1}^{j-1} \mathbf{X}_i \right| + \ln |\mathbf{X}_j| - j \ln \left| \sum_{i=1}^j \mathbf{X}_i \right| \}. \end{aligned} \quad (2)$$

The  $R_j$  constitute a factorization of  $Q$ , i.e.,

$$\ln Q = \sum_{j=2}^k \ln R_j. \quad (3)$$

The distributions of the  $-2 \ln Q$  and  $-2 \ln R_j$  test statistics under the assumption of no change are approximately  $\chi^2$  with  $(k-1)f$  and  $f = p_1^2 + p_2^2 = 2$  degrees of freedom, respectively. Better approximations for dual and full polarization data (for the full matrix case) are given in [1].

With this method we build a structure of change for each pixel: first we look at change over all time points, then at change over all time points omitting the first time point, then at change over all time points omitting the first two time points, etc. The change structure is illustrated in Table 1 (where we illustrate with six time points). Note

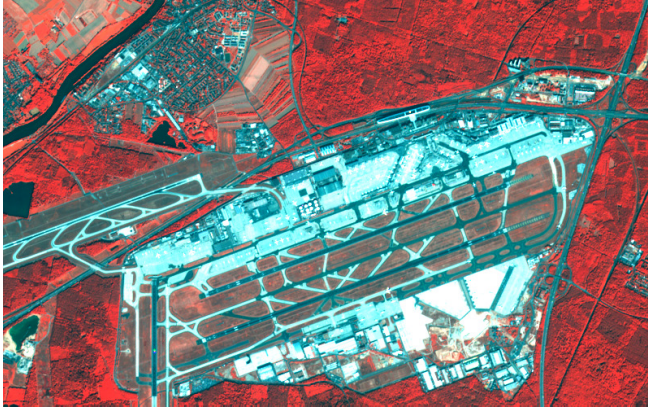


**Fig. 1.** RGB image of Sentinel-2 MSI band 4 (near-infrared as R), band 3 (red as G), and band 2 (green as B), 10 m pixels, 5 km north-south and 8 km east-west, Frankfurt Airport, Germany, acquired on 12 Sep 2016.

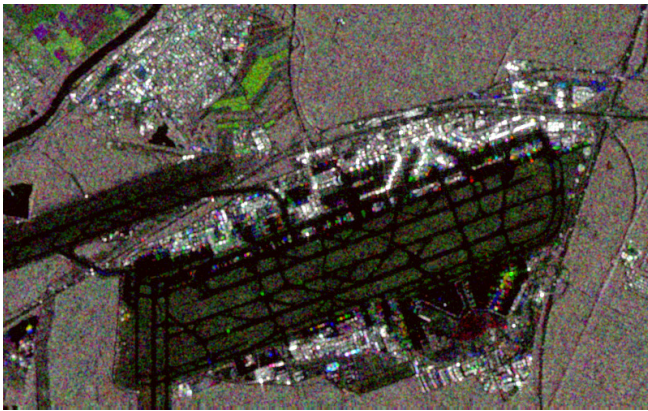


**Fig. 2.** RGB image of Sentinel-1 C-band multi-temporal VH data, 10 Feb 2016 as R, 9 Jun 2016 as G, and 12 Nov 2016 as B, 10 m pixels, 5 km north-south and 8 km east-west, all three bands are stretched linearly between  $-24$  dB and 0 dB.

that the pairwise tests for comparison between  $t_i$  and  $t_{i+1}$ ,  $R_2^{(i)}$ , appear on the diagonal.

If a change is detected comparing for example  $t_2$  and  $t_3$  in the “ $t_1 = \dots = t_6$ ” column in Table 1, the remaining tests in that column are invalid and we continue in the column starting with detection of change from  $t_3$ . This will leave the “ $t_2 = \dots = t_6$ ” column irrelevant. Continuing like this we can build up the change pattern for all pixels over all time points, see also [1, 8].

### 3. S1 (AND S2) DATA, FRANKFURT AIRPORT

The data used in this study are from the Sentinel-1 dual polarization (here VV/VH, diagonal only) C-band SAR instrument. 19 scenes (all ascending node and all with relative orbit number 15) covering the international airport in Frankfurt, Germany, are obtained from Google Earth Engine<sup>2</sup> (GEE) [9]. They cover the time span 10

<sup>2</sup><https://earthengine.google.com> and <https://developers.google.com/earth-engine>.



**Fig. 3.**  $-2 \ln Q$  omnibus change detector for Sentinel-1 C-band VV/VH dual polarization data, diagonal only, over 19 time points from 10 Feb 2016 through 12 Nov 2016, stretched linearly between 0 and 200.

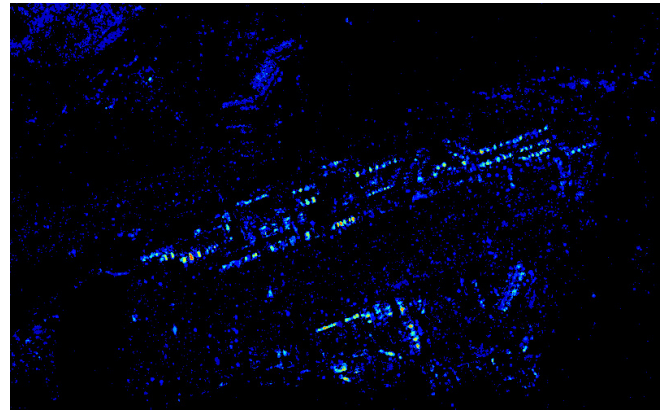


**Fig. 4.** Number of changes (change frequency map) detected by  $R_j$  in Sentinel-1 C-band VV/VH dual polarization data, diagonal only, over 19 time points from 10 Feb 2016 through 12 Nov 2016.

Feb 2016 – 12 Nov 2016. The data acquired in instrument Interferometric Wide Swath (IW) mode, are S1 Ground Range Detected (GRD) scenes, processed using the Sentinel-1 Toolbox<sup>3</sup> to generate a calibrated, ortho-corrected product. This processing includes thermal noise removal, radiometric calibration, and terrain correction using Shuttle Radar Topography Mission 30 m (SRTM 30) data. Finally it includes saturating the data (quoting GEE): “Values are then clamped to the 1st and 99th percentile to preserve the dynamic range against anomalous outliers, and quantized to 16 bits.” This is to avoid excessive precision loss during conversion from floats to integers for storage. The outliers are usually due to strong reflections from sharp angles on antennas and other man-made objects. The spatial resolution is (range by azimuth) 20 m by 22 m and the pixel spacing is 10 m. The IW data are multi-looked, the number of looks is 5 by 1 and the equivalent number of looks is 4.9.

To give a good visual impression of the area Figure 1 shows an RGB image of bands 4, 3, and 2 (near-infrared, red, and green) from

<sup>3</sup><https://sentinel.esa.int/web/sentinel/toolboxes/sentinel-1>.

the Sentinel-2<sup>4</sup> MultiSpectral Instrument (MSI), level-1C processed, 500 by 800 10 m pixels. These data acquired on 12 Sep 2016 are obtained from GEE also.

Figure 2 shows an RGB representation of the VH data from 10 Feb (red), 9 Jun (green), and 12 Nov (blue), again 500 by 800 10 m pixels.

#### 4. RESULTS

Figure 3 shows the  $-2 \ln Q$  omnibus change detector for Sentinel-1 C-band VV/VH dual polarization, diagonal only data over 19 time points from 10 Feb 2016 through 12 Nov 2016. No-change regions have low values of  $-2 \ln Q$ , appear dark, and coincide mostly with wooded areas. Change regions have high values of  $-2 \ln Q$ , appear bright, and are primarily due to aircraft coming and going to and from gates and aprons in the airport. Also some change is associated with agricultural activities to the north and the north-west of the airport near the town of Kelsterbach.

Figure 4 shows the number of changes detected by  $R_j$  over the 19 time points. We also term this a change frequency map. There are up to 15 changes at the significance level chosen, change probability 0.9999 (corresponding to a no-change probability 0.0001). High change frequencies occur where aircraft come and go at the gates and where aircraft park on aprons. Low change frequencies occur in agricultural fields. No change occurs mostly in wooded areas.

To demonstrate the validity of the  $\chi^2$  approximation for the  $-2 \ln Q$  and  $-2 \ln R_j$  test statistics, Figure 5 shows histograms for an analysis of omnibus change for the first ten time points (10 Feb through 15 Jul 2016) along with the theoretical distributions for a no-change wooded area. For all the  $-2 \ln R_j$  the number of degrees of freedom is 2, for the  $-2 \ln Q$  the numbers of degrees of freedom are 18, 16, ..., 2, respectively. Judged visually the histograms and the theoretical distributions fit nicely. The structure in the figure is the same as in Table 1.

Saturating the extreme pixel values as done in GEE is unfortunate in our situation where the dominating changes detected are due precisely to those strongly reflecting man-made objects mentioned in Section 3, namely aircraft. Pixels that are saturated at several time points may not be detected as change pixels, which is potentially wrong. The best way to handle this is to store the data as floats but of course this would double the amount of storage required in the GEE data archive. Further, the Wishart distribution applied is valid in principle only for fully developed speckle which we do not have for aircraft. This led us to perform a small test (not shown here) where we had the same Sentinel-1 data as here for three time points over a military aircraft graveyard at the Davis-Monthan Air Force Base in Tuscon, Arizona, USA. As opposed to results from the analysis in this paper, the non-moving aircraft in the three time point case were not detected as change. This gives us confidence in the validity of the results described in this paper.

#### 5. SOFTWARE

Matlab and Python code to perform this kind of analysis is available [8].

#### 6. CONCLUSIONS

The omnibus analysis in a satisfactory fashion points to areas of high change in the S1 data over the 19 time points, namely where aircraft

come and go at the airport's gates and aprons. It also shows some change in agricultural regions. Finally the theoretical distributions of the test statistics in a no-change region fit nicely with their experimental histograms.

Storing the data in 16 bits with saturation of extreme pixels to avoid loss of dynamics as done in Google Earth Engine is unfortunate. This is especially true in this case where the most conspicuous change is associated with high and therefore saturated values.

The Wishart distribution is not ideal for man-made objects such as aircraft. However, based on a small study with stationary aircraft we have confidence in the results obtained.

The ability of the method to detect and isolate regions of intense activity, together with the ongoing availability of Sentinel imagery, suggest applications in the area of remote monitoring, for example in the verification of arms control and disarmament agreements.

#### 7. REFERENCES

- [1] K. Conradsen, A. A. Nielsen, and H. Skriver, "Determining the points of change in time series of polarimetric SAR data," *IEEE Transactions on Geoscience and Remote Sensing*, vol. 54, no. 5, pp. 3007–3024, May 2016, <http://www.imm.dtu.dk/pubdb/p.php?6825>.
- [2] J. J. van Zyl and F. T. Ulaby, "Scattering matrix representation for simple targets," in *Radar Polarimetry for Geoscience Applications*, F. T. Ulaby and C. Elachi, Eds. Artech, Norwood, MA, 1990.
- [3] K. Conradsen, A. A. Nielsen, J. Schou, and H. Skriver, "A test statistic in the complex Wishart distribution and its application to change detection in polarimetric SAR data," *IEEE Transactions on Geoscience and Remote Sensing*, vol. 41, no. 1, pp. 4–19, Jan. 2003, <http://www.imm.dtu.dk/pubdb/p.php?1219>.
- [4] J. Schou, H. Skriver, A. A. Nielsen, and K. Conradsen, "CFAR edge detector for polarimetric SAR images," *IEEE Transactions on Geoscience and Remote Sensing*, vol. 41, no. 1, pp. 20–32, Jan. 2003, <http://www.imm.dtu.dk/pubdb/p.php?1224>.
- [5] M. J. Canty, *Image Analysis, Classification and Change Detection in Remote Sensing, with Algorithms for ENVI/IDL and Python*, Taylor & Francis, CRC Press, third revised edition, 2014.
- [6] A. A. Nielsen, K. Conradsen, and H. Skriver, "Change detection in full and dual polarization, single- and multi-frequency SAR data," *IEEE Journal of Selected Topics in Applied Earth Observations and Remote Sensing*, vol. 8, no. 8, pp. 4041–4048, Aug. 2015, <http://www.imm.dtu.dk/pubdb/p.php?6827>.
- [7] V. Akbari, S. N. Anfinsen, A. P. Doulgeris, T. Eltoft, G. Moser, and S. B. Serpico, "Polarimetric SAR change detection with the complex Hotelling-Lawley trace statistic," *IEEE Transactions on Geoscience and Remote Sensing*, vol. 54, no. 7, pp. 3953–3966, July 2016.
- [8] A. A. Nielsen, K. Conradsen, H. Skriver, and M. J. Canty, "Visualization of and software for omnibus test based change detected in a time series of polarimetric SAR data," *Submitted*, 2017, <http://www.imm.dtu.dk/pubdb/p.php?6962>.
- [9] Google Earth Engine Team, "Google Earth Engine: A planetary-scale geo-spatial analysis platform," <https://earthengine.google.com>, 12 2015.

<sup>4</sup><https://sentinel.esa.int/web/sentinel/missions/sentinel-2>.

**Table 1.** Illustration of the change structure for an example with data from six time points.

	$t_1 = \dots = t_6$	$t_2 = \dots = t_6$	$t_3 = \dots = t_6$	$t_4 = \dots = t_6$	$t_5 = t_6$
Omnibus	$Q^{(1)}$	$Q^{(2)}$	$Q^{(3)}$	$Q^{(4)}$	$Q^{(5)}$
$t_1 = t_2$	$R_2^{(1)}$				
$t_2 = t_3$	$R_3^{(1)}$	$R_2^{(2)}$			
$t_3 = t_4$	$R_4^{(1)}$	$R_3^{(2)}$	$R_2^{(3)}$		
$t_4 = t_5$	$R_5^{(1)}$	$R_4^{(2)}$	$R_3^{(3)}$	$R_2^{(4)}$	
$t_5 = t_6$	$R_6^{(1)}$	$R_5^{(2)}$	$R_4^{(3)}$	$R_3^{(4)}$	$R_2^{(5)}$

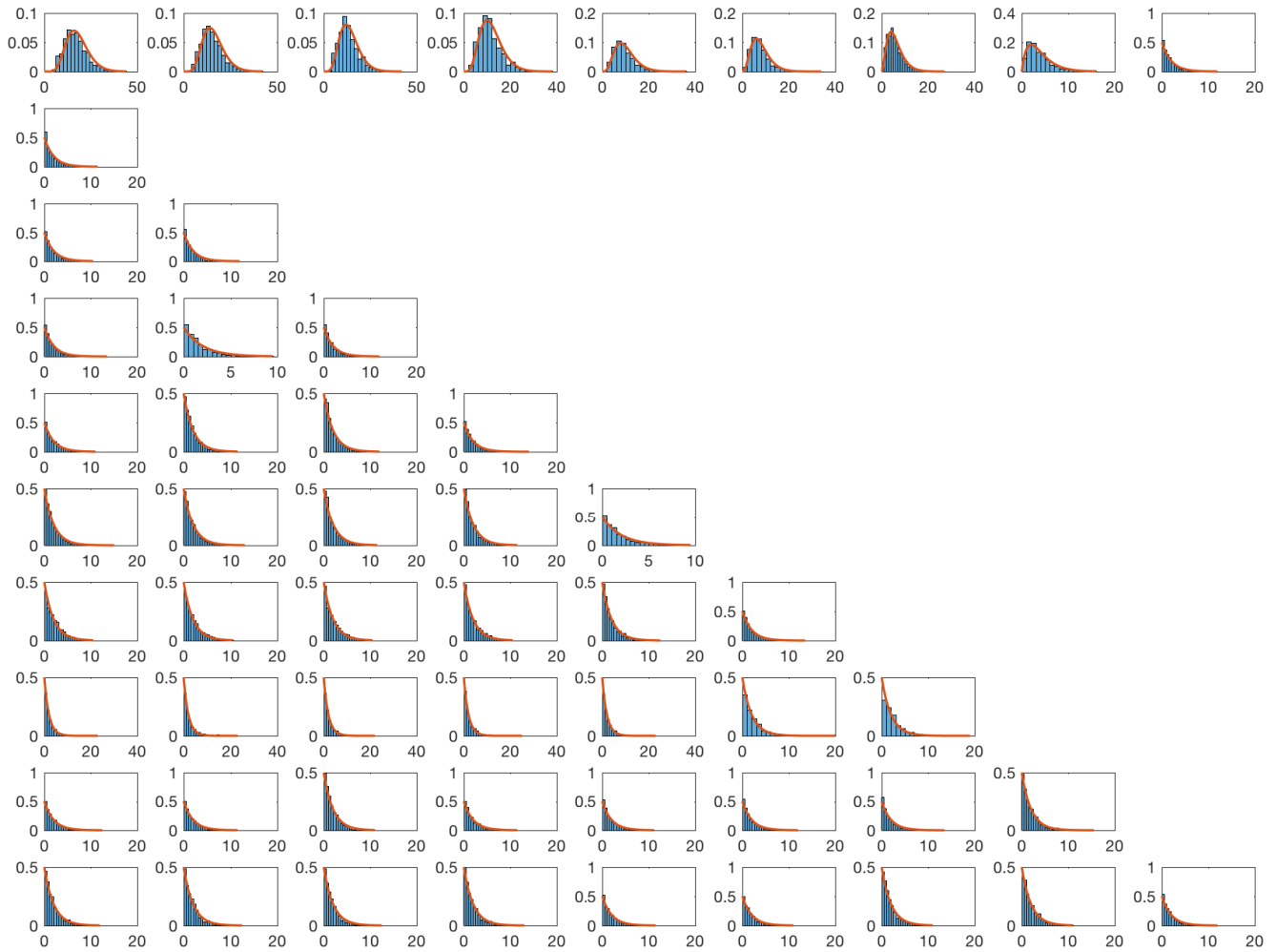


**Fig. 5.** Histograms for an analysis of omnibus change for the first ten time points of the Sentinel-1 data (10 Feb through 15 Jul) along with the theoretical distributions for a no-change wooded area. For the  $-2 \ln Q$  (top row plots) the numbers of degrees of freedom are 18, 16, ..., 2, respectively. For all the  $-2 \ln R_j$  (the remaining rows) the number of degrees of freedom is 2. Judged visually this illustrates a satisfactory fit between sample histograms and theoretical distributions for the test statistics in a no-change region. The structure in this figure is the same as in Table 1.